Flows induced in a cylinder with both end walls rotating

Daniel T. Valentine and Craig C. Jahnke

Citation: Physics of Fluids **6**, 2702 (1994); doi: 10.1063/1.868159
View online: http://dx.doi.org/10.1063/1.868159
View Table of Contents: http://scitation.aip.org/content/aip/journal/pof2/6/8?ver=pdfcov
Published by the AIP Publishing

Flows induced in a cylinder with both end walls rotating

Daniel T. Valentine and Craig C. Jahnke
Department of Mechanical and Aeronautical Engineering, Clarkson University, Potsdam, New York 13699-5725

(Received 18 February 1994; accepted 29 April 1994)

The flow field inside a cylindrical container induced by the rotation of the top and bottom end walls with a fixed sidewall is described. For this problem, this paper shows that stagnation points occur along the axis of rotation between the midplane of symmetry and the rotating end walls for appropriate values of the characteristic parameters, viz., the Reynolds number and the aspect ratio of the container. Aspect ratios of 0.5, 0.8, 1.0, and 1.5 were examined over a range of Reynolds numbers from 100 to 2000. As the Reynolds number increased beyond a critical value a recirculation zone surrounding a columnar vortex core in the meridional-plane flow pattern is predicted to occur near the midplane. This toroidal vortex is different from the type B vortex breakdown phenomenon that occurs in cylindrical containers with only one end wall rotating.

I. INTRODUCTION

In this paper the internal flows induced by rotating the end walls of a cylinder with a fixed sidewall are examined. Three classes of problems that lead to steady solutions in cylindrical containers with rotating end wall(s) and/or a rotating sidewall are (1) the flow induced by rotating the top end wall at rotation rate Ω; (2) the flow induced by rotating the top end wall at Ω_1, the side wall at Ω_2 and the bottom end wall at Ω_3 such that $\Omega_1<\Omega_2<\Omega_3$; and (3) the flow induced by rotating the top and bottom end walls at Ω with the sidewall fixed at zero. The first problem has an extensive literature because under appropriate conditions internal vortex breakdown phenomena are known to occur. The second problem has not been investigated to the same extent; however, it has some interesting features that have been reported in the literature. The third problem is investigated in this paper by computational means. The discussion of the results includes a comparison with related experimental data that have been reported in the literature. The literature on the first two problems provides some helpful guidance in interpreting the results for the third problem.

The observations of flows induced by a rotating end wall reported by Vogel[1,2] and Ronnenberg[3] were extended substantially by Escudier.[4] Not only did Escudier reproduce the single-bubble vortex breakdown observed by Vogel and Ronnenberg, he also mapped regions of two-bubble and three-bubble breakdowns, as well as regions of oscillatory solutions in the parameter space of Reynolds number versus container aspect ratio. The structure of the single-bubble vortex breakdown phenomenon observed in the flow inside the cylinder is a type B breakdown as described by Leibovich.[5] Another significant feature of these flows is that they are predominantly axisymmetric. Hence, computational investigations that solve the axisymmetric equations of motion provide useful information about the details of these flows.

The computational study of Lugt and Haussling[6] provides a preliminary glimpse into the onset of vortex breakdown in a cylinder caused by a rotating end wall. Lugt and Abboud[7] extended this study and included the effects of thermal gradients to within the Boussinesq approximation. Neitzel[8] examined the motion of streaklines in the interpretation of numerical results and made comparisons with flow visualization data. Lopez,[9] Brown and Lopez,[10] and Lopez and Perry[11] describe the results of an extensive numerical investigation of the rotating end-wall problem. They presented comparisons with the experimental observations reported by Escudier,[4] described the physical mechanism of the breakdown phenomenon in these flows, and described the details of two unsteady modes of motion (periodic internal separation and coalescence of bubbles). Daube and Sorensen[12] and Tsitverbilt[13] suggest that the unsteady modes occur at a supercritical Hopf bifurcation as Reynolds number is increased beyond a critical value for the aspect ratio $AR=H/R=2.5$, where H is the height of the cylinder and R is its radius. This conjecture is plausible because Escudier[4] did not find hysteresis at the location of the critical Reynolds number (he approached the critical value from above and below in his experimental investigation).

The physical mechanism of the vortex breakdown as described by Brown and Lopez[10] is caused by an excess centrifugal force at the stationary end wall which induces an overshoot that leads to a centrifugal wave. The divergence of streamlines, which forms a stationary wave pattern (near the vortex core), produces negative azimuthal vorticity. This negative azimuthal vorticity induces an opposing meridional flow along the axis of symmetry that ultimately causes a stagnation point to occur on the axis of symmetry.

Hyun[14] investigated the effects of different rotation rates applied to the top end wall, the sidewall and the bottom end wall. At large times (approaching steady state) Hyun predicted that the meridional circulation in the interior consists of a purely vertical flow that moves from the end wall rotating at the slower speed towards the end wall rotating at the faster speed. The side wall in his study rotated at a rate intermediate of the two end walls.

Spohn, Mory and Hopfinger,[15] and Spohn[16] studied the flow induced by rotating the bottom end wall of a cylinder with a fixed sidewall and a free surface. This flow is analogous to the flow in the lower half-plane of a cylinder with both end walls rotating at the same rate if the free surface is nearly flat and surface tension effects are negligible; in this case, the free surface acts as a pure slip boundary. Spohn

 1070-6631/94/6(8)/2702/9/$6.00

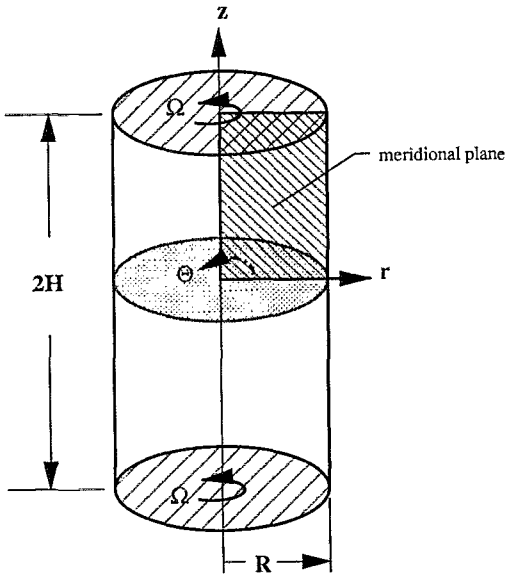

FIG. 1. Illustration of flow-field geometry.

et al. found that recirculation bubbles occur for certain combinations of aspect ratio and Reynolds number and mapped regions of single and double vortex breakdowns and the boundary between steady and unsteady flow. Roesner[17] studied the flow in a cylinder with both end walls rotating and a fixed sidewall. He showed that a slight co-rotation of the second end wall tends to enhance the occurrence of recirculation bubbles while a slight counter-rotation of the second end wall tends to suppress formation of recirculation bubbles.

From the literature we find that in a cylindrical container with one or both end walls rotating and a fixed sidewall, vortex breakdown phenomena occur for certain combinations of the aspect ratio and Reynolds number. In this paper we examine the recirculation bubbles (or "vortex-breakdown" phenomena) that occur in flows in cylindrical containers when both end walls are rotated at the same rate with a fixed sidewall. Significant changes are observed in the flow field when the aspect ratio and Reynolds number are varied. We show that the type of vortex breakdown that occurs is different from the well-known internal-flow vortex breakdown that is predicted in the problem with only one end wall rotating. Steady-state solutions for various combinations of Reynolds number and aspect ratio are presented and discussed. Comparisons are also made with the results of Spohn, Mory and Hopfinger.[15]

II. COMPUTATIONAL ANALYSIS

The geometry of the flow field analyzed in this study is illustrated in Fig. 1. The flow field driven by rotating the end walls is assumed to be axisymmetric. The equations describing the axisymmetric flow inside the cylindrical container are the equations for the azimuthal component of the vorticity, ω, the azimuthal component of the velocity (or swirl), v, and the meridional-plane streamfunction, ψ. The model equations are

$$\frac{\partial \omega}{\partial t}+\frac{1}{r}\frac{\partial ur\omega}{\partial r}+\frac{\partial w\omega}{\partial z}=2\frac{v}{r}\frac{\partial v}{\partial z}+\frac{u\omega}{r}+\frac{1}{\mathrm{Re}}\left(\frac{\partial^2\omega}{\partial r^2}+\frac{1}{r}\frac{\partial \omega}{\partial r}-\frac{\omega}{r^2}+\frac{\partial^2\omega}{\partial z^2}\right), \tag{1}$$

$$\frac{\partial v}{\partial t}+\frac{1}{r}\frac{\partial urv}{\partial r}+\frac{\partial wv}{\partial z}+\frac{uv}{r}=\frac{1}{\mathrm{Re}}\left(\frac{\partial^2 v}{\partial r^2}+\frac{1}{r}\frac{\partial v}{\partial r}-\frac{v}{r^2}+\frac{\partial^2 v}{\partial z^2}\right), \tag{2}$$

$$\frac{\partial^2\psi}{\partial r^2}-\frac{1}{r}\frac{\partial \psi}{\partial r}+\frac{\partial^2\psi}{\partial z^2}=r\omega, \tag{3}$$

where

$$u=\frac{1}{r}\frac{\partial \psi}{\partial z}, \quad w=-\frac{1}{r}\frac{\partial \psi}{\partial r}, \tag{4}$$

and

$$\omega=\frac{\partial u}{\partial z}-\frac{\partial w}{\partial r}.$$

The u is the radial component of velocity and the w is the vertical component of velocity. The dimensionless parameter in Eqs. (1) and (2) is the Reynolds number, defined as

$$\mathrm{Re}=\Omega R^2/\nu,$$

where ΩR is the characteristic velocity, R is the characteristic length scale, and ν is the kinematic viscosity of the fluid inside the cylinder. Because axisymmetric flow is assumed, the computations were done on an equally spaced $M\times N$ finite-difference grid in the meridional plane. The boundary condition imposed on all of the surfaces of the cylindrical container surrounding the fluid is the no-slip condition. In all but two of the computed cases a midplane of symmetry condition was imposed at the midplane between the top and bottom end walls; hence, most of the computations were done in the upper half of the meridional plane.

Two computational methods were applied in this investigation. Since steady-state solutions are of primary interest, the first method applied solved for steady-state solutions only. The steady solutions were calculated as follows. Equation (4) was used to write Eqs. (1)–(3) in terms of ψ, v, and ω only. Steady solutions of the resulting equations are determined by setting all of the time derivatives equal to zero, discretizing the resulting partial differential equations and then applying a continuation method to the discretized equations. Second-order central differences are used to discretize the partial differential equations except at the boundaries where first-order differences are used.

The discretized system has the form

$$f(\mathbf{x};\mathrm{Re})=0, \tag{5}$$

where f is a system of $3NM$ equations, $\mathbf{x}$ is a $3NM$ dimensional vector representing the discretized values of ψ, v, and ω. Equation (5) is solved using a pseudo-arclength continuation technique based on the work of Doedel and Kernevez[18] that has previously been used by Jahnke and Culick[19,20] to study nonlinear aircraft dynamics and nonlinear acoustics in

combustion chambers. The Reynolds number is used as the continuation parameter, so steady solutions are obtained for a range of Reynolds numbers at a fixed aspect ratio.

The second method was used to solve initial-value problems. Initial conditions used were (i) for $t<0$ the fluid is at rest (or at a steady-state determined with the continuation method), (ii) for $t\geqslant 0$ both end walls of the cylinder are instantaneously set into a rotating motion at the angular speed of Ω (or are maintained in motion at Ω). The evolution of the flow field is computed until a steady-state condition is approached (or a transition to a new state is computed). A steady state was determined to have been reached when the *sum* over all of the grid points of the absolute value of the partial derivative with respect to time of the azimuthal vorticity was less than unity.

The temporal evolution of ω and v described by Eqs. (1) and (2), respectively, was computed by applying the ETUDE-IN-R scheme developed by Valentine[21] and recently applied by Valentine and Miller[22] to spin-up and spin-down problems in cylindrical containers. This scheme is a finite-difference approximation that is first order in time and nearly second order in space. It is a low-order scheme that was designed to significantly reduce the false diffusion truncation error. The Poisson-like equation, viz., Eq. (3), was written in terms of second-order central differences and solved by successive overrelaxation at each time step to determine ψ. For further details on the application of this time-dependent scheme to solve internal flow problems in cylindrical containers, including favorable comparisons with experimental data of spin-up from rest and computations of the single rotating end wall flow, the reader is referred to the paper by Valentine and Miller.[22]

The two computational methods were used in a complementary way in the present work. The continuation procedure is very effective in providing steady solutions as a function of one of the parameters of the system, but the procedure is computationally intensive as Newton's method is used, requiring matrix inversions. The matrix inversion limits the size of problems that can be solved in a reasonable time. Continuation results presented in this paper were obtained for a grid size of 1/60. Convergence studies done for grid sizes of 1/40, 1/50, and 1/60 showed convergence for a grid spacing of 1/60 for Reynolds numbers less than 2000. Lopez[9] also found that a grid size of 1/60 was sufficient for this range of Reynolds numbers for the single rotating lid problem. As a further check on the accuracy of the continuation solutions, time dependent computations were run with a grid spacing of 1/120 using the continuation solution as an initial condition. No significant differences were observed between the two sets of results. The time dependent computations were also used to determine the stability of steady states obtained with the continuation method.

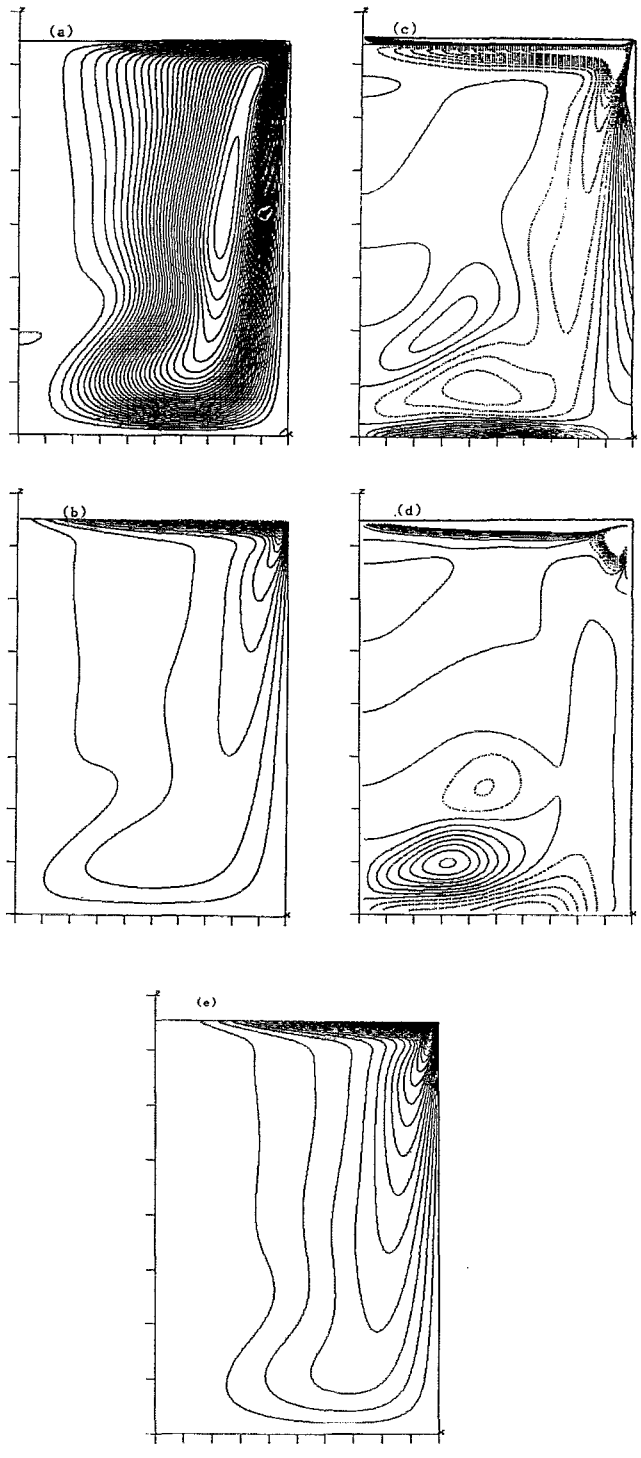

FIG. 2. Contour plots for the flow induced by a rotating top wall and fixed bottom and sidewalls, Re=1854, $AR=1.5$. (a) Streamlines, $-0.008<\psi<0.0025$, $\Delta\psi=0.00025$. (b) Swirl, $0\leqslant v<1.0$, $\Delta v=0.05$. (c) Azimuthal vorticity, $-2<\omega\leqslant 0$ (——), $0<\omega<2$ (···), $\Delta\omega=0.2$. (d) $\Lambda=(v^2/r-\partial P/\partial r)$, $-0.04<\Lambda<0$ (···), $0\leqslant\Lambda<0.04$ (——), $\Delta\Lambda=0.004$. (e) $\Gamma=rv$, $0<\Gamma<1.0$, $\Delta\Gamma=0.025$.

III. RESULTS AND DISCUSSION

The motivation for this study came from studying the flow field illustrated in Fig. 2. This is a computational reproduction of one of the flow fields investigated experimentally by Escudier.[4] It is the steady flow induced by a rotating end wall (in this case the top end wall) with Re=1854 and $AR=1.5$. The figure presents contour plots in the meridional plane of the streamlines, ψ, the swirl, v, the azimuthal vorticity, ω, the imbalance between the centrifugal force and radial pressure gradient, $\Lambda\equiv(-\partial P/\partial r+v^2/r)$, where $P\equiv p/(\rho R^2\Omega^2)$ is the dimensionless pressure, and the angu-

lar momentum, $\Gamma \equiv rv$. The streamline pattern shows a single recirculation region (or breakdown bubble) on the central axis of the flow field just below the vertical location of $z=0.4$ above the fixed (or bottom) end wall of the container. Its size, shape, and location compare favorably with the flow visualization data reported by Escudier for this case.

The flow in Fig. 2 is driven by the rotating top lid. Angular momentum is imparted to the fluid as it moves through the Ekman layer along the top wall. As the fluid moves through the sidewall boundary layer it loses angular momentum. It continues to lose angular momentum when it turns the corner and moves through the bottom (fixed-wall) boundary layer. As the fluid flows through the bottom boundary-layer towards the cylinder axis ($r=0$) its swirl velocity tends to increase as the fluid attempts to conserve angular momentum. Near the sidewall ($r=1$) and adjacent to the entire bottom boundary Λ is less than zero as illustrated in Fig. 2(d). This causes the radial component of the velocity of the fluid particles to increase as they move from the side wall region towards the axis of the container. Fluid particles accelerate towards the axis of the container until Λ starts to increase, resulting in a decrease in the radial velocity. Along the contours where Λ changes sign the radial velocity is a local maximum or a local minimum depending upon whether the local pressure gradient exceeds the local centrifugal force ($\Lambda<0$) or is less than the local centrifugal force ($\Lambda>0$), respectively.

In the bottom boundary layer Λ is initially negative. When Λ changes sign the streamlines turn clockwise, towards the top end wall and ultimately towards the sidewall. Subsequently, the sign of Λ changes again in the direction along the streamline causing the streamline to turn counterclockwise, upward and back towards the axis of the cylinder. This undulating motion of the fluid as it moves upward is easily observed in Fig. 2(a). This stationary wave pattern in the streamlines is strong enough, in this case, to induce a recirculating region along the central axis. The stagnation points at the leading and trailing edge of the bubble are inside the region where the azimuthal vorticity is negative; it is this vorticity that induces the stagnation points, as described by Brown and Lopez.[10]

It is the waviness of the streamlines that causes the wavyness in the swirl pattern (as swirl is transported along streamlines) which results in finite values of vorticity production due to the term $(2v/r)(\partial v/\partial z)$ in the vorticity equation, Eq. (1). This term changes sign as z increases; thus, near the largest undulations between the bottom end wall and the middle of the meridional plane, a local maximum of the azimuthal vorticity is followed by a local minimum of the azimuthal vorticity as shown in Fig. 2(c). It is the vorticity adjacent the recirculation bubble that plays the dominant role in the locally induced meridional velocity field in this region as is easily demonstrated by an examination of the Biot–Savart Law (see Brown and Lopez[10]).

The fact that the occurrence of stagnation points along the central axis away from the lids is possible is also reflected in the equation of continuity; when the radial velocity changes in magnitude and direction in the meridional plane, the vertical velocity must change as well. Near the breakdown bubble the stationary inertial wave is relatively large in amplitude. The initial rebound of the fluid expunged from the bottom boundary layer causes the fluid to move in the positive r direction; hence, the vertical velocity is significantly diminished. This reduction in vertical velocity signals the potential onset of a breakdown bubble in the core flow. This type of separation bubble has been described by Leibovich[5] as a type B vortex breakdown phenomenon. This flow field is quite well known. Hence, further discussion of it will only be made when necessary for comparison with the flows described next.

We raised the following question: How would the flow field change if the boundary condition on the nonrotating end wall of the flow field illustrated in Fig. 2 was pure-slip instead of no-slip? The experimental configuration that could produce this alternative situation is a container twice as tall with both end walls rotating at the same rate and in the same direction. If a midplane symmetry condition is invoked to solve for the flow field in the upper half of the meridional plane, then this is the configuration posed in the question. It is this problem that we solved with the assumption that a pure-slip rigid-wall condition can be applied at the midplane of symmetry. A related flow is the flow with the bottom end wall rotating and the upper boundary a free surface as in Spohn *et al.*[15] If the free-surface shape is nearly flat and surface tension effects are negligible, the free-surface boundary may be modeled the same way as the midplane of symmetry boundary condition. Thus, if an appropriately defined Froude number is small enough, the problem with bottom rotating lid and free surface is essentially the same as the problem investigated in this paper.

The steady streamline pattern for this problem with $\mathrm{Re}=1854$ and $AR=1.5$, where the aspect ratio is now the half-height divided by the radius of the cylinder, is illustrated in Fig. 3. It is evident that the flow field of this problem is quite different from that of the flow field in Fig. 2. The new flow field has four distinct regions; the Ekman layers along the end walls of the cylinder, a concentrated vortex core along the central axis with negligible axial and radial motion, an annular region surrounding the core with significantly larger secondary flow, and a toroidal pair of vortices that surround the core (the pair includes the image on the other side of the midplane). Figure 5(d) in Spohn *et al.*,[15] showing the streaklines for $AR=1.5$ and $\mathrm{Re}=2095$, shows a toroidal vortex attached to the free surface which agrees qualitatively with the streamlines shown in Fig. 3(a). Because there is no decrease in angular momentum associated with wall shear stresses along the bottom wall (or midplane of symmetry) in this case, the "overshoot" in the swirl of the fluid particles that causes the streamlines to turn upward, occurs at a larger radius as compared with the flow in Fig. 2.

There are, however, comparable features of the flows in Figs. 2 and 3. Several features in Fig. 2 appear to be rotated counterclockwise to a new location in Fig. 3. For example, the stagnation points in Fig. 2 correspond to the periodic points on the midplane in Fig. 3 (which are points where $u=w=0$ but v is finite and hence points on the dividing stream surface between the outer flow and the recirculatory flow in the toroidal vortices). Another example is the loca-

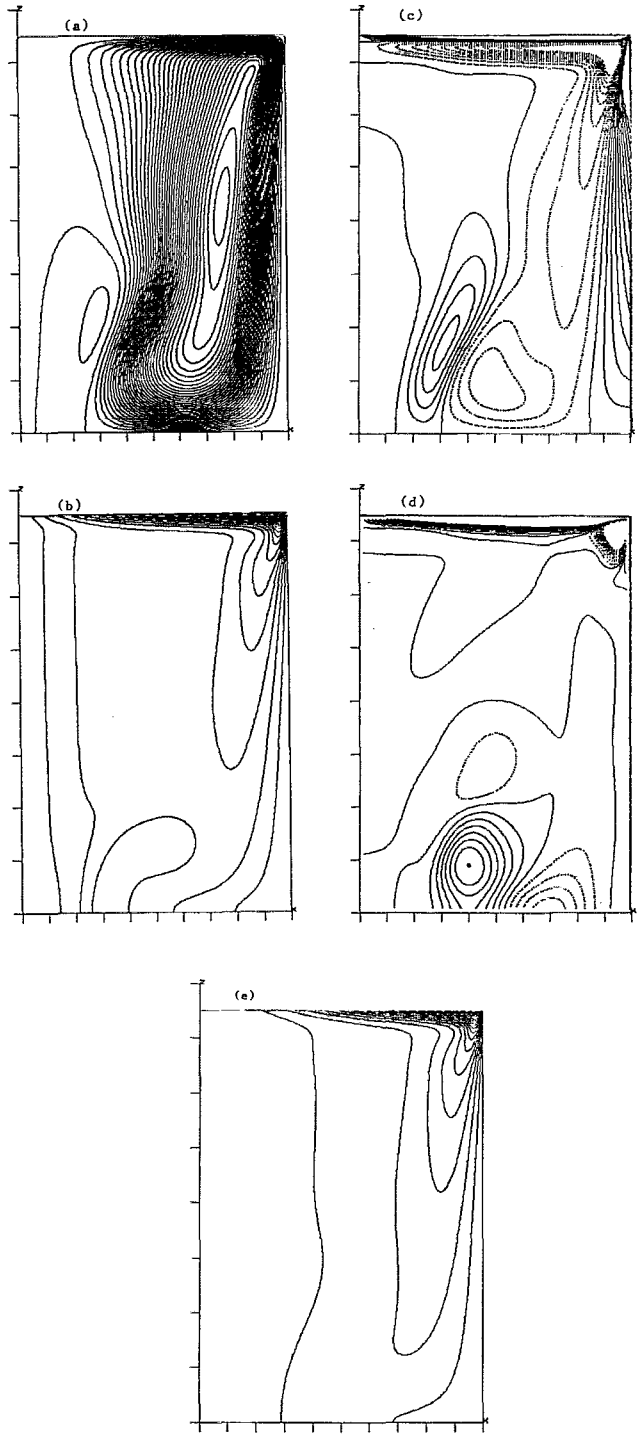

FIG. 3. Contour plots for the flow induced by a rotating-top end wall, pure-slip (plane of symmetry) bottom surface, and fixed sidewall, Re=1854, $AR=1.5$. (a) Streamlines, $-0.0085<\psi<0.0005$, $\Delta\psi=0.0005$. (b) Swirl, $0\leqslant v<1.0$, $\Delta v=0.05$. (c) Azimuthal vorticity, $-2<\omega\leqslant 0$ (——), $0<\omega<2$ (···), $\Delta\omega=0.2$. (d) $\Lambda=(v^2/r-\partial P/\partial r)$, $-0.04<\Lambda<0$ (···), $0\leqslant\Lambda<0.04$ (——), $\Delta\Lambda=0.004$. (e) $\Gamma=rv$, $0<\Gamma<1.0$, $\Delta\Gamma=0.05$.

tion of the regions of opposite signed values of Λ. In Fig. 3 the spatial extent of the regions containing the local maximum and local minimum values of Λ are smaller and nearer the corner of the midplane and the sidewall. The major structures in the contours of azimuthal vorticity are also shifted in a counterclockwise direction.

The recirculation bubble in Fig. 3 is a toroidal (or ring) vortex as compared with the breakdown bubble in Fig. 2. Since the structure of this flow field is quite different from the flows investigated by Escudier,[4] Lopez,[9] Brown and Lopez,[10] and Lopez and Perry,[11] among others, and since it depends on Re and AR, we sought to map the regions in this parameter space where qualitative changes in the streamline pattern are predicted to occur and to describe some of the details of the solutions in each region. Table I summarizes the cases we computed. By applying the continuation method described in the previous section we systematically varied Re and AR to investigate the changes in steady-state solutions in this parameter space. We determined the occurrence of a recirculation zone on the central axis, its migration towards the midplane and its detachment from the central axis onto the midplane, resulting in a toroidal vortex surrounding a concentrated cylindrical vortical core. This same sequence of events is reported in Spohn *et al.*[15]

The locations of the stagnation and/or periodic points that mark the leading and trailing edges of the recirculatory region along the centerline of the cylinder ($r=0$) and through the midplane ($z=0$) are shown in Fig. 4 as functions of Re for $AR=0.5$, 0.8, 1.0, and 1.5. Positive values of the ordinate correspond to the location of a stagnation point along the axis of the cylinder ($r=0$), while negative values of the ordinate correspond to periodic points on the midplane ($z=0$). The trajectories in Fig. 4 indicate that a recirculation bubble first occurs on the central axis at a critical Reynolds number. For aspect ratios of 1.0 and 1.5 the recirculation bubble initially occurs as a slender bubble demarcated by a streamline that terminates at two stagnation points on the axis of the cylinder. This elongated vortex is similar to the slender vortex predicted by Leibovich[23] based on an extension of slender-body theory. For an aspect ratio of 0.5 the initial recirculation bubble is demarcated by a streamline that terminates at a stagnation point on the axis of the cylinder and a periodic point on the midplane. Thus it seems that low aspect ratio containers preclude the existence of a slender recirculation bubble on the axis of the cylinder. Even for the cases where the slender recirculation bubble exists on the axis of the cylinder it only persists for a narrow range of Reynolds numbers; this range increases with increasing aspect ratio.

The slender recirculation bubble on the axis of the cylinder disappears when the lower stagnation point crosses over the stagnation point at $(r,z)=(0,0)$ and becomes a periodic point of the flow. This flow structure is seen to persist over a relatively large range of Reynolds numbers. The remaining stagnation point on the axis of the cylinder experiences a rapid change in location at a critical Reynolds number. At this critical value of Re the pressure gradient near $r=0$ on the midplane changes sign as the stagnation point on the axis of the cylinder becomes a periodic point on the midplane. Thus, the recirculation region forms a toroidal vortex that surrounds a concentrated axial vortex. As shown in Fig. 4 the size of this central-core vortex increases with Reynolds number (at least for the range of Reynolds numbers

TABLE I. Summary of cases.

Case	Re	AR[a]	$M\times N$	Computational domain	Bottom lid B.C.
			A: Continuation calculations		
1	100→3000	0.5	61× 31	upper half-plane	symmetry plane
2	100→2000	0.8	61× 49	upper half-plane	symmetry plane
3	100→2000	1.0	61× 61	upper half-plane	symmetry plane
4	100→3000	1.5	61× 91	upper half-plane	symmetry plane
			B: ETUDE-in-R calculations		
5	1854	1.5	121×181	entire meridional plane	no-slip, $\Omega=0$
6	1854	1.5	121×181	upper half-plane	symmetry plane
7	760	1.5	121×181	upper half-plane	symmetry plane
8	1300	1.5	121×181	upper half-plane	symmetry plane
9	2000	1.5	121×181	upper half-plane	symmetry plane
10	2000	1.0	61×121	entire meridional plane	no-slip, $\Omega=0.9\ \Omega_{top}$
11	2000	1.0	61×121	entire meridional plane	no-slip, $\Omega=\Omega_{top}$
12	3000	1.5	61× 91	upper half-plane	symmetry plane

[a]The aspect ratio is based on the half-height of the container for all cases except case 5, where the aspect ratio is based on the entire height of the container.

examined in the present study). This same trend is noted in the experimental results of Spohn *et al.*[15]

For aspect ratios of 0.5 and 0.8 a second recirculation bubble is found to occur at a critical value of the Reynolds number. The second recirculation bubble occurs on the cylinder axis inside the cylindrical vortical core that is surrounded by the toroidal vortex. As the Reynolds number is further increased the second recirculation bubble moves off the cylinder axis resulting in a flow with two toroidal vortices in the upper half-plane of symmetry. Spohn *et al.*[15] do not report observing multiple recirculation bubbles for $AR=0.5$. However, one reason may be the difficulties reported by Spohn *et al.*[15] in introducing dye into the bubble region without disturbing the recirculating flow for $AR<1$. As a result, they introduced dye at the corner of the rotating end wall and the sidewall for $AR<1$ flows, but were then unable to get dye into the core region for $AR<0.5$.

Figure 5 summarizes the critical combinations of Re and AR delineating the onset of these changes in the flow field; sketches of the streamline patterns of the recirculation bubbles in the corresponding regions of (Re, AR) parameter space are also shown. The results of Spohn *et al.*[15] regarding the critical Reynolds number for the onset of a recirculation bubble agree with the current results for $AR\geqslant 1$, but do not agree with the current results for $AR<1$. For $AR<1$ the current results show that the Reynolds number for the onset of the recirculation bubble decreases with decreasing AR, while Spohn *et al.*[15] predict that the Reynolds number for the onset of the recirculation bubble increases with decreasing AR. Flow visualization difficulties or possible free-surface effects (as the Froude number increases with decreasing AR and increasing Reynolds number) at low AR could account for the differences evident for $AR<1$.

For a given aspect ratio, say $AR=1.5$, as the Reynolds

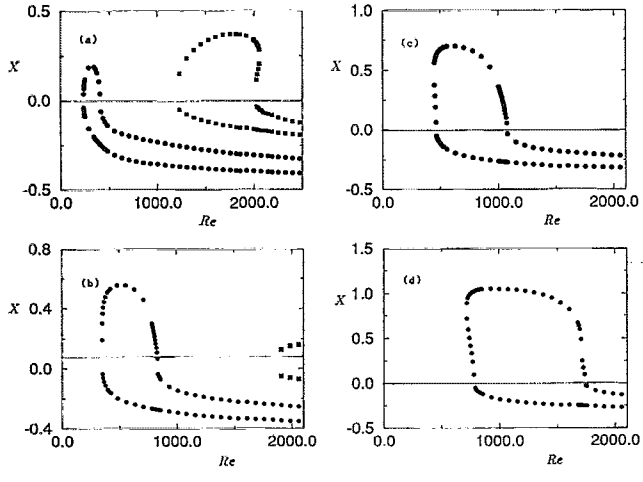

FIG. 4. The locations of the stagnation points on $r=0$ and the periodic points on the midplane ($z=0$) as functions of Reynolds number, $X=z|_{r=0}$, $X=-r|_{z=0}$. (a) $AR=0.5$, (b) $AR=0.8$, (c) $AR=1.0$, (d) $AR=1.5$.

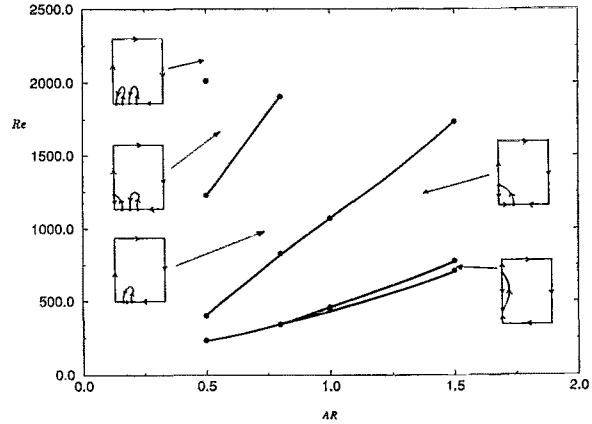

FIG. 5. Curves in (Re, AR) parameter space where transitions occur in the locations of the stagnation points and periodic points attached to the recirculation bubble(s) for flows in a cylindrical container with top and bottom end walls rotating at the same rate and a fixed sidewall. The illustrations are cartoons of the recirculation bubble(s) in the upper half of the meridional plane.

number is increased from Re≈100 there is a series of changes that occur in the flow pattern. The first change is the appearance of an elongated recirculation bubble along the central axis between the end wall and midplane at Re=750. Figure 6 presents the streamline pattern, the swirl distribution, the azimuthal component of the vorticity, the imbalance between the centrifugal force and radial pressure gradient, and the angular momentum for $AR=1.5$ and Re=760. This case illustrates more precisely, the geometry of the flow pattern when the recirculation zone occurs on the central axis; for this case there are two stagnation points that occur between the midplane and the end wall. There is, of course, another stagnation point on the midplane at $r=0$. Streamlines for this case compare favorably with Fig. 5(b) from Spohn *et al.*[15] where Re=770.

As Reynolds number is increased, the slender recirculation bubble moves toward the midplane. The recirculation bubble moves toward the midplane because the amplitude of the centrifugal wave increases with Re while the wavelength decreases (cf. Figs. 3 and 6). Negative azimuthal vorticity produced by the centrifugal wave thus becomes stronger and moves toward the midplane as Re increases. Since it is this negative azimuthal vorticity that brings the flow to rest on the axis of the cylinder creating the stagnation points, one would expect the stagnation points, and thus the recirculation bubble, to migrate toward the midplane with increasing Re.

At a particular value of Re the stagnation point closest to the midplane passes over the stagnation point on the midplane at $r=0$ and ceases to be a stagnation point for the flow; it becomes a periodic point. The meridional velocity is zero at this point, but the swirl is nonzero. Figure 7 illustrates the flow pattern for this situation; it presents the streamlines, the swirl distribution, the azimuthal vorticity, the imbalance between the centrifugal force and radial pressure gradient, and the angular momentum contours for $AR=1.5$, Re =1300. Streamlines for this case compare qualitatively with Fig. 5(c) from Spohn *et al.*[15] where Re=975. Note that the current results predict this type of recirculation bubble for 780<Re<1730. We observe that the meridional flow separates at a point on the midplane at $r\approx0.2$. At this point $u=w=0$ and $v\approx0.1$. The dividing streamline intersects the axis of the cylinder at $z\approx1.0$ at a stagnation point ($u=v=w=0$). The reverse flow along the central axis near the midplane is induced primarily by the meridional vorticity adjacent to this location. (Recall Fig. 3, which presents the details of the flow for $AR=1.5$ and Re=1854 and the previous discussion of this flow. This represents the case when a toroidal vortex exist around a central axial vortex.)

The question of whether or not the qualitative features of the flow change when the symmetry condition about the midplane is relaxed was also examined. Figure 8(a) presents the streamline pattern for Re=2000 with $AR=1.0$ (based on the half-height) when the lower lid is rotating at 90% of the rotation rate of the upper lid. Asymmetry in the top and bottom halves of the meridional plane are indeed observed; however, the gross features of the pattern are quite similar to the symmetric flow. The solution for Re=2000 with $AR=1.0$ (based on the half-height) when the lower lid is rotating at the same rotation rate, as the upper lid is shown in Fig. 8(b). Note that symmetry was not assumed in this case, the entire flow field was calculated. Hence, the predicted flow fields are rather robust and should easily be observed experimentally.

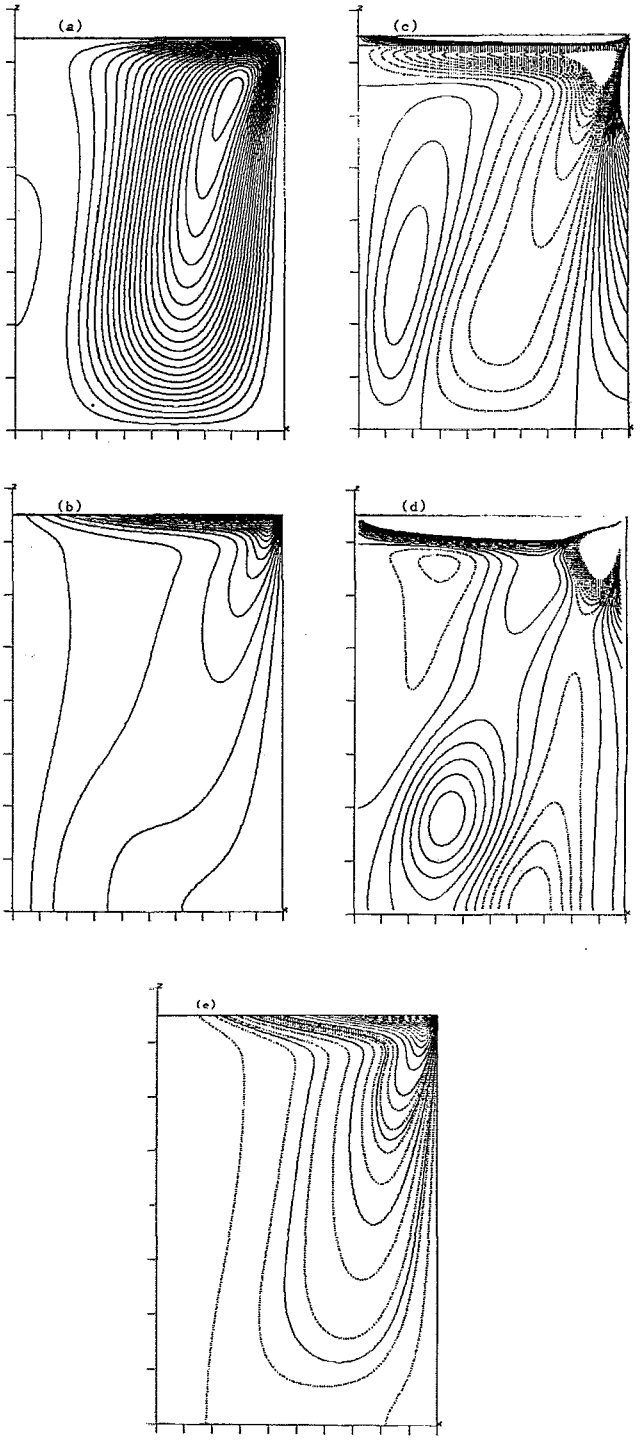

FIG. 6. Contour plots for the flow induced by a rotating-top end wall, pure-slip (plane of symmetry) bottom surface, and fixed sidewall, Re=760, $AR=1.5$. (a) Streamlines, $-0.011<\psi<0.0005$, $\Delta\psi=0.0005$. (b) Swirl, $0\leq v<1.0$, $\Delta v=0.05$. (c) Azimuthal vorticity, $-1.5<\omega\leq0$ (——), $0<\omega<1.5$ (···), $\Delta\omega=0.1$. (d) $\Lambda=(v^2/r-\partial P/\partial r)$, $-0.015<\Lambda<0$ (···), $0\leq\Lambda<0.0015$ (——), $\Delta\Lambda=0.001$. (e) $\Gamma=rv$, $0<\Gamma<1.0$, $\Delta\Gamma=0.02$ (···), $\Delta\Gamma=0.05$ (——).

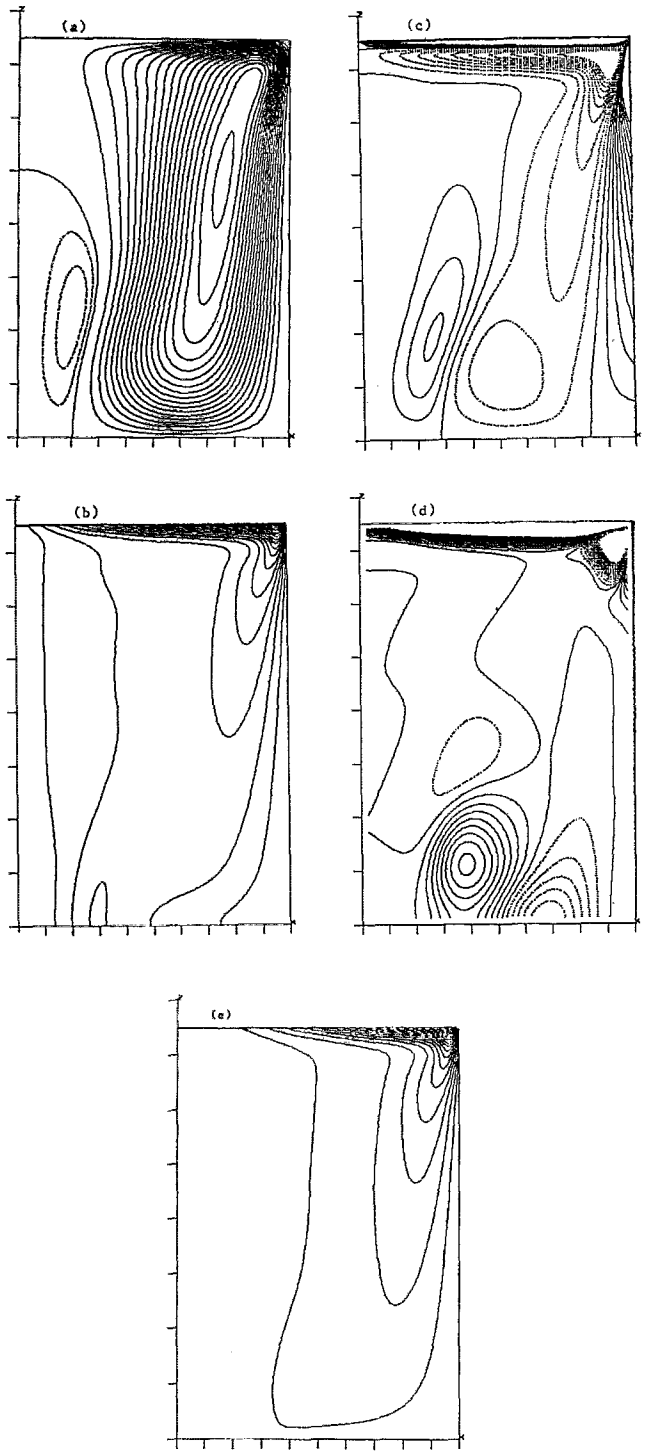

FIG. 7. Contour plots for the flow induced by a rotating-top end wall, pure-slip (plane of symmetry) bottom surface, and fixed sidewall, Re=1300, $AR=1.5$. (a) Streamlines, $-0.01<\psi\leq 0$ (——), $\Delta\psi=0.0005$, $0<\psi\leq 0.0005$ (···), $\Delta\psi=0.0001$. (b) Swirl, $0\leq v<1.0$, $\Delta v=0.05$. (c) Azimuthal vorticity, $-2.0<\omega\leq 0$ (——), $0<\omega<2.0$ (···), $\Delta\omega=0.2$. (d) $\Lambda=(v^2/r-\partial P/\partial r)$, $-0.04<\Lambda<0$ (···), $0\leq\Lambda<0.04$ (——), $\Delta\Lambda=0.004$. (e) $\Gamma=rv$, $0<\Gamma<1.0$, $\Delta\Gamma=0.05$.

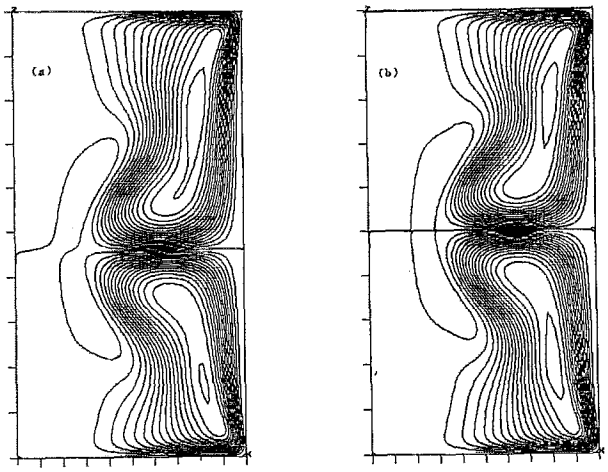

FIG. 8. Illustration of the effect of a difference in rotation rate between the top and bottom end walls with fixed sidewall, Re=2000, $AR=1.0$. Contours of streamlines for (a) $\Omega_{Top}=1.0$, $\Omega_{Bottom}=0.9$, $-0.0085<\psi<0.008$, $\Delta\psi=0.0005$. (b) $\Omega_{Top}=\Omega_{Bottom}=1.0$, $-0.0085<\psi<0.0085$, $\Delta\psi=0.0005$.

Finally, the possible existence of oscillatory solutions was examined by computing a solution for Re=3000 and $AR=1.5$. For this case, we found that the steady-state solution determined with the continuation method is unstable and that a stable oscillatory solution exists. This Reynolds number was selected because it was thought to be above the critical value where unsteady solutions are expected to occur; this is because oscillatory solutions for the case of one rotating end wall were found by Escudier[4] to exist for Reynolds numbers above 2700, and for the case of a rotating bottom end wall with a free surface were found by Spohn *et al.*[15] to exist for Reynolds numbers above 2200. Figure 9(a) shows the time trace of the streamfunction at $(r,z)=(\frac{1}{6},\frac{1}{3})$. The Fourier transform of this signal is presented in Fig. 9(b) and shows that the frequency content of the oscillation consists

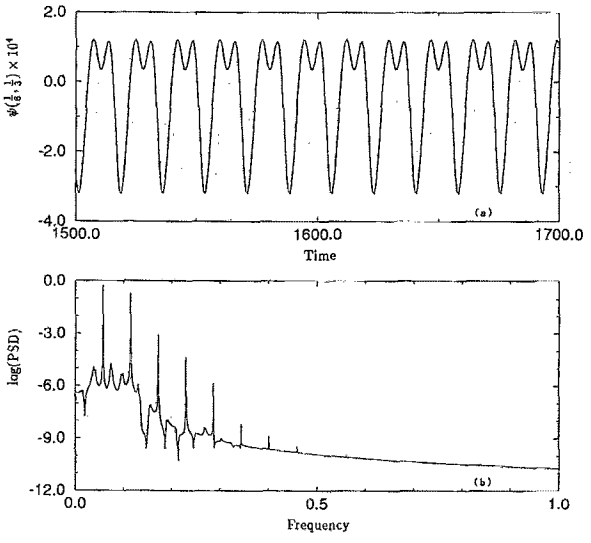

FIG. 9. Example of oscillatory motion in a container with top and bottom end walls rotating at equal rates with fixed sidewall, Re=3000, $AR=1.5$. (a) Streamfunction at $(r,z)=(\frac{1}{6},\frac{1}{3})$. (b) FFT of this signal for $880<t<1700$ with sampling time $\Delta t=0.1$ (which is ten times the computational time step).

of a fundamental frequency, $f_1 \approx 0.0574$ Hz, and its corresponding harmonics.

To summarize, we have shown that recirculation bubbles occur in cylindrical containers with both end walls rotating at the same rate and a stationary sidewall for certain combinations of Reynolds number and aspect ratio. Several types of recirculation bubbles have been found. For high aspect ratio containers and relatively low Reynolds numbers slender recirculation bubbles appear on the axis of the cylinder. At higher Reynolds numbers the recirculation bubble moves towards the midplane, eventually forming a toroidal vortex around an axial vortex core. These results compare favorably with the experimental results of Spohn *et al.*[15] for $AR \geqslant 1$. We also have found that multiple toroidal vortices occur for low aspect ratio containers. The overall structure of this flow is reasonably robust as illustrated by comparison with the flow field induced by rotating the top and bottom end walls at somewhat different rates. Finally, the existence of oscillatory solutions has also been demonstrated.

ACKNOWLEDGMENTS

Partial funding for this work was provided by the National Science Foundation under Grant No. INT-8819665 and the National Aeronautics and Space Administration under Grant No. OSP-5039, which is the grant that supports a graduate student and summer fellowships for undergraduates to participate in research in science and engineering under the Clarkson Space Grant Program which is part of the New York Space Grant Consortium administered by Cornell University.

[1]H. U. Vogel, "Experimentelle Ergebnisse über die laminare Strömung in einem zylindrischen Gehäuse mit darin rotierender Scheibe," Max-Planck-Inst. Strömungsforschung, Göttingen, Bericht **6** (1968).

[2]H. U. Vogel, "Rückströmungsblasen in Drallströmungen." Festschrift 50 Jahre Max-Planck-Inst. Strömungsforschung, Göttingen, Bericht, 1925–1975 (1975).

[3]B. Ronnenberg, "Ein selbstjustierendes 3-Komponenten-Laserdoppleranemometer nach dem Vergleichsstrahlverfahren, angewandt für Untersuchungen in einer stationären zylinder-symmetrischen Drehströmung mit einem Rückstromgebiet," Max-Planck-Inst. Strömungsforschung, Göttingen, Bericht **20** (1977).

[4]M. P. Escudier, "Observations of the flow produced in a cylindrical container by a rotating end wall," Exp. Fluids **2**, 189 (1984).

[5]S. Leibovich, "Vortex stability and breakdown: Survey and extension," AIAA J. **22**, 1192 (1984).

[6]H. J. Lugt and H. J. Haussling, "Axisymmetric vortex breakdown in rotating fluid within a container," Trans. ASME E: J. Appl. Mech. **49**, 921 (1982).

[7]H. J. Lugt and M. Abboud, "Axisymmetric vortex breakdown with and without temperature effects in a container with a rotating lid," J. Fluid Mech. **179**, 179 (1987).

[8]G. P. Neitzel, "Streak-line motion during steady and unsteady axisymmetric vortex breakdown," Phys. Fluids **31**, 958 (1988).

[9]J. M. Lopez, "Axisymmetric vortex breakdown. Part 1. Confined swirling flow," J. Fluid Mech. **221**, 533 (1990).

[10]G. L. Brown and J. M. Lopez, "Axisymmetric vortex breakdown. Part 2. Physical mechanisms," J. Fluid Mech. **221**, 533 (1990).

[11]J. M. Lopez and A. D. Perry, "Axisymmetric vortex breakdown. Part 3. Onset of periodic flow and chaotic advection," J. Fluid Mech. **234**, 449 (1992).

[12]O. Daube and J. N. Sorensen, "Simulation numérique de l'écoulement périodique axisymétrique dans une cavité cylindrique," C. R. Acad. Sci. Paris **308**, 463 (1989).

[13]N. Tsitverblit, "Vortex breakdown in a cylindrical container in the light of continuation of a steady solution," Fluid Dyn. Res. **11**, 19 (1993).

[14]J. M. Hyun, "Spin-up from rest in a differentially rotating cylinder," AIAA J. **21**, 1278 (1983).

[15]A. Spohn, M. Mory, and E. J. Hopfinger, "Observations of vortex breakdown in an open cylindrical container with a rotating bottom," Exp. Fluids **14**, 70 (1993).

[16]A. Spohn, "Ecoulement et éclatement tourbillonaires engendré par une disque tournant dans une enceinte cylindrique," Thèse de Doctorat d'Université, Université Joseph Fourier Grenoble I, March, 1991.

[17]K. G. Roesner, "Recirculating zones in a cylinder with rotating lid," in *Topological Fluid Mechanics*, Proceedings of the IUTAM Symposium, Cambridge, 1989, edited by K. Moffat and A. Tsinober (Cambridge University Press, London, 1990).

[18]E. J. Doedel and J. P. Kernevez, "Software for continuation problems in ordinary differential equations with applications," preprint, California Institute of Technology, Pasadena, California, 1985.

[19]C. C. Jahnke and F. E. C. Culick, "Application of bifurcation theory to the high-angle-of-attack dynamics of the F-14," J. Aircraft **31**, 26 (1994).

[20]C. C. Jahnke and F. E. C. Culick, "An application of dynamical systems theory to non-linear combustion instabilities," to appear in J. Propul. Power.

[21]D. T. Valentine, "Computational analysis of spin-up from rest of a stably-stratified fluid in a cylinder," ASME Comput. Engin. **I**, 631 (1992).

[22]D. T. Valentine and Miller, "Generation of ring vortices in axisymmetric spin-down: A numerical investigation," Phys. Fluids **6**, 1535 (1994).

[23]S. Leibovich, "Axially-symmetric eddies embedded in a rotational stream," J. Fluid Mech. **32**, 529 (1968).